International Journal of Nanoelectronics and Materials
IJNeaM
ISSN 1985-5761 | E-ISSN 2232-1535

Effect of infill density and re-carbon black loading on the electrical and mechanical properties of epoxy-filled 3D printed structures

Yahmunaa Javerseetharaman[a], Cheow Keat Yeoh [a,b]*, Pei Leng Teh [b], Chong Hooi Yew [c], Chun Hong Voon [d], Nor Azura Abdul Rahim [a], and Halimatuddahliana Nadutionand [e]

[a]*Faculty of Chemical Engineering Technology, Universiti Malaysia Perlis*
[b]*Frontier Materials Research Centre of Excellence (FrontMate), Universiti Malaysia Perlis (UniMAP), Perlis, Malaysia*
[c]*Ecopower Synergy Sdn. Bhd., 1A, Jalan Kenari 9, Bandar Puchong Jaya, 47100 Puchong, Selangor*
[d]*Institute of Nano Electronic Engineering, Universiti Malaysia Perlis, Lot 106, 108 & 110, Blok A, Taman Pertiwi Indah, Jalan Kangar-Alor Setar, Seriab, Perlis, Kangar, 01000, Malaysia*
[e]*Department of Chemical Engineering, Faculty of Engineering, Universitas Sumatera Utara, Padang Bulan, Medan 20155, Indonesia*
∗Corresponding author. e-mail: ckyeoh@unimap.edu.my

Received 10 May 2026, Revised 25 May 2026, Accepted 5 June 2026

ABSTRACT

This study investigates the additive effect of recycled carbon black (rCB) loading from 0 to 3 wt% and infill densities of 50%, 70% and 90% on the multifunctional performance of hybrid polymer composites. Polylactic Acid (PLA) samples were produced using Fused Deposition Modeling (FDM) with diverse interior geometries and subsequently infilled with an insulating epoxy resin to strengthen structural integrity. Mechanical evaluation using tensile and Vickers microhardness testing indicates that a 90% infill density offers the most effective structural framework, with a 3 wt% rCB loading resulting in the highest ultimate tensile strength (UTS) of 21.9 MPa. Significantly, although mechanical strength was generally enhanced with increased infill, 100% dense structures displayed reduced efficiency attributable to thermal stress and insufficient layer adhesion. Electrical characterization via impedance spectroscopy reveals a non-monotonic behavior; while 2 wt% rCB approaches the percolation threshold for conductive pathways, a "dielectrically blocking" phenomenon arises at 3 wt% rCB, where resistance reaches a maximum of 1.0×10^11 Ω due to particle agglomeration. The study indicates that 2 wt% rCB yields a significant 104.6% enhancement in ductility compared to pure PLA at 50% infill. These findings define a method for the development of cost-effective, high-strength smart materials appropriate for sensing applications.

Keywords: *Carbon black, Recycled carbon black, PLA composites, Electrical conductivity, Impedance spectroscopy, 3D printing, Epoxy infilling*

1. INTRODUCTION

Three-dimensional (3D) printing, specifically Fused Deposition Modeling (FDM), has become a revolutionary manufacturing technique for fabricating intricate, layer-by-layer geometries from digital models. Polylactic Acid (PLA) is the most widely used thermoplastic in this processing method due to its high printability, eco-friendliness, and adequate prototyping strength. However, the inherent insulating properties of PLA limit its use in electronic components and smart systems. To overcome this limitation, conductive fillers [1], such as recycled carbon black (rCB), are integrated to enable the development of charge-conducting channels within the polymer matrix. Recovered from the pyrolysis of end-of-life tires, rCB functions as a sustainable and economical substitute for conventional virgin carbon fillers.

An essential yet inadequately explored factor in the development of these multifunctional materials is the interaction between infill density and internal post-processing treatment. Infill density determines the interior microstructure, material continuity, and void fraction of the printed specimen. Although its function in reducing weight and improving mechanical performance is documented, its impact on altering electrical properties—such as conductivity and dielectric behavior when the internal voids are filled with a secondary phase like epoxy resin—remains a significant research gap. Epoxy infiltration is employed to improve interfacial bonding and overall density, transforming a hollow 3D-printed shell into a fully dense composite.

The primary thesis of this study is that the synergy between internal lattice geometry and conductive filler loading governs the transition from semi-insulating to functional conductive regimes. By systematically varying CB content and infill density in epoxy-filled PLA structures, this research aims to optimize the balance between structural load-bearing capacity and electrical functionality.

2. THEORETICAL BACKGROUND

The efficacy of 3D-printed composites is primarily based on percolation theory and the Maxwell-Wagner-Sillars (MWS) effect. Percolation defines the minimum filler concentration

necessary to create a continuous conductive network; for carbon black-reinforced polymers, this threshold is strongly influenced by particle dispersion and the geometric limitations of the 3D-printed scaffold. Infill density directly affects this by modifying material continuity and void volume. Increased densities diminish porosity, thereby improving filler dispersion and promoting the establishment of conductive channels.

The introduction of an insulating substance such as epoxy into the conductive PLA/CB structure does not enhance electrical conductivity, but instead modifies the dielectric environment and creates tunnel barriers between conductive clusters. In multi-phase 3D-printed scaffolds, the MWS effect arises as charge carriers build up at the internal interfaces between the conductive CB particles and the insulating epoxy core due to the differences in their dielectric constants.

Moreover, the mechanical integrity of these systems is regulated by the "shell-core" connection. Research indicates that although increased infill percentages often enhance tensile strength up to an optimal threshold, totally dense (100%) infill structures may experience thermal stress accumulation or incomplete layer fusion, leading to a reduction in mechanical performance. Thus, the 90% infill configuration is theorized to provide the ideal balance for epoxy penetration and load distribution.

3. METHODOLOGY

The manufacturing process followed a multi-phase experimental design comprising raw material compounding, filament extrusion, 3D printing, and epoxy infiltration.

3.1. Raw Material and Filament Preparation

The matrix material used in this experiment was PLA powder purchased from NatureWorks (Ingeo 3310), while the conductive filler, recycled carbon black (rCB), was supplied by Ecopower, Kuala Lumpur. Conductive filaments were produced by compounding PLA powder with 1, 2, and 3 wt% rCB using a twin-screw extrusion method. The extrusion temperature profile ranged from 160°C at the feed zone to 180°C at the die, with a constant screw speed of 60 rpm to ensure homogeneous mixing of the matrix and filler. The produced filament maintained a standard diameter of 1.75±0.05 mm. A two-component, room-temperature-curing epoxy resin (Epoxy Malaysia, Selangor), characterized by a Shore hardness of 84 and a flexural strength of 28 kg/mm^2, was utilized as an infill for the PLA/CB-based 3D-printed samples.

3.2. 3D Printing and Internal Geometry

Testing specimens were designed in a dumbbell shape according to the standard ASTM D638 Type V. The specimens were designed and the printing parameters were configured using Ultimaker Cura slicing software. The samples were then printed at three different infill densities: 50%, 70%, and 90%. A standard rectilinear (grid) pattern was applied to the specimens to maintain a consistent pore geometry.

The structural shell parameters were characterized by a wall thickness of 0.8 mm and a top/bottom thickness of 0.8 mm. The samples were printed in a flat, horizontal orientation using a fixed layer height of 0.2 mm. Extrusion was executed at a printing temperature of 220°C and a constant print speed of 40 mm/s.

3.3. Epoxy Infiltration and Post-Processing

The epoxy resin, based on diglycidyl ether of bisphenol A (DGEBA), was combined with an amine-based hardener in a 3:1 weight ratio. This mixture was manually applied to the 3D-printed samples, allowing it to infiltrate the internal lattice under ambient conditions. The samples were then cured at room temperature for 36 hours to ensure complete curing.

4. DATA COLLECTION AND ANALYSIS

The characteristics of the PLA/CB-based 3D-printed samples infilled with epoxy composite were evaluated through several tests.

4.1. Mechanical Characterization

Tensile properties, specifically the ultimate tensile strength, Young's modulus, and elongation at break, were measured using a Universal Testing Machine (UTM) at a constant crosshead speed of 2.5 mm/s. Each formulation was tested with 7 replicates to ensure statistical significance. In addition to tensile properties, surface hardness was evaluated using the Vickers Microhardness Test (ASTM E384) by applying a force of 9.8 N for a dwell time of 10 seconds to minimize viscoelastic creep during testing.

4.2. Electrical Characterization

Electrical impedance was measured using the Hioki IM3536 Impedance Analyzer. An alternating voltage of 1 V was applied over a frequency range of 10 Hz to 10 kHz. Conductive silver paste was applied to the specimens before testing to guarantee optimal electrode contact during testing.

4.3. Morphological and Chemical Analysis

The evolution of chemical integration and functional groups present in the composite was analyzed using Fourier Transform Infrared (FTIR) spectroscopy with a scan range of 4000 cm^{-1} to 400 cm^{-1}. Microstructural characteristics were studied using Optical Microscopy (OM) at a magnification of 5X to gain insight into the resin and particle distribution within the surface of the infilled specimens.

5. RESULTS AND DISCUSSION

5.1. Mechanical Properties

Table 1. Mechanical Properties of PLA_CB composite with Epoxy infill

Sample Group	Infill Density (%)	Tensile Strength (MPa)	Young's Modulus (MPa)	Elongation at Break (%)
Pure PLA	50	13.6±0.55	301±27.6	23.7±2.49
	70	15.9±0.58	372±12.1	21.4±0.87
	90	18.6±0.45	418±13.9	19.9±0.62
	100	15.2±3.27	315±81.8	43.1±14.6
CB1	50	14.3±0.86	249±11.6	36.5±4.47
	70	16.1±0.88	240±6.49	22.2±1.72
	90	15.0±0.34	237±8.22	17.2±2.00
	100	10.8±0.97	224±18.7	35.1±5.24
CB2	50	15.1±0.70	251±10.4	48.5±3.32
	70	15.0±0.94	249±18.8	27.8±1.71
	90	18.6±0.39	307±9.74	32.3±2.09
	100	14.3±1.68	304±8.21	32.4±2.65
CB3	50	16.1±0.17	279±17.8	20.1±0.95
	70	18.6±0.49	281±10.5	16.5±1.06
	90	21.9±0.46	314±9.39	24.5±2.97
	100	13.3±1.78	246±33.5	23.5±1.49

5.1.1. Tensile Strength

The experimental findings demonstrate that infill density significantly affects the mechanical properties of 3D-printed samples (Figure 1), with PURE PLA samples showing a progressive increase in strength from 13.6 MPa (50%) to 18.6 MPa (90%). This trend aligns with the understanding that higher infill percentages improve load-bearing capacity up to an optimal threshold [1]. Nonetheless, the samples with 100% density exhibited a significant reduction in strength, indicating potential issues with thermal stress accumulation or inadequate layer fusion in dense structures [2].

The integration of rCB modifies this behavior depending on the concentration. At a minimal loading of 1 wt%, rCB particles act primarily as stress concentrators, compromising the continuity of the PLA matrix and impeding the sintering process [3]. This resulted in a 19.4% decrease in tensile strength for the CB1 sample at 90% infill compared to PURE PLA. In contrast, the CB3 samples achieved the highest performance across all densities, peaking at 21.9 MPa at 90% infill. This suggests that at 3 wt%, the rCB particles attain sufficient proximity to establish percolating networks that connect printed layers and facilitate efficient load transfer [3].

5.1.2. Young's Modulus and Stiffness Behavior

Young's modulus (Figure 2) for PURE PLA followed a similar density-dependent trend, reaching a maximum of 418 MPa at 90% density before decreasing in the 100% dense state. The incorporation of 1 wt% resulted in an unexpected decrease in stiffness, ranging from 17% to 29% across all densities. These drops occurred because the rCB particles interfered with the long-range polymer phase and induced matrix discontinuity.

A partial recovery of stiffness was observed at higher rCB loadings. As shown in the graph, the CB3 samples reached a modulus of 314 MPa at 90% density, achieving 75% of the PURE PLA sample stiffness. This recovery indicates that elevated concentrations are able to enhance the efficacy of filler-matrix interactions and particle-to-particle reinforcement. The reduction in modulus at 100% density across all categories indicates that fully dense structures experience processing-induced flaws, such as residual stress or modified crystallinity, which outweigh the benefits of maximum material content.

5.1.3. Elongation at Break and Toughening Mechanisms

The elongation behavior (Figure 3) displayed a significantly non-linear pattern, where the pure PLA samples exhibited an unexpected increase in ductility at 100% density (43.1). This is likely due to the elimination of void-related stress concentration sites [4]. The most notable discovery was the remarkable ductility of CB2 samples at 50% density, which exhibited a 104.6% increase compared to pure PLA. The enhancement in toughness is ascribed to mechanisms including crack deflection, particle debonding, and matrix shear yielding, which dissipate energy via numerous micro-failure events [5, 6].

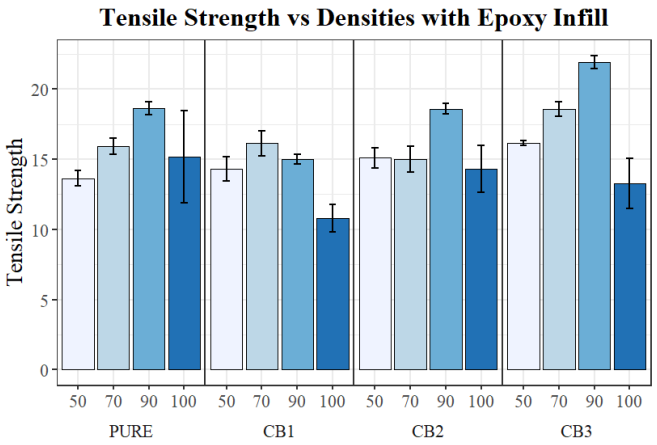

Figure 1. Variation of ultimate tensile strength as a function of infill density for pure and CB-reinforced PLA/Epoxy composites

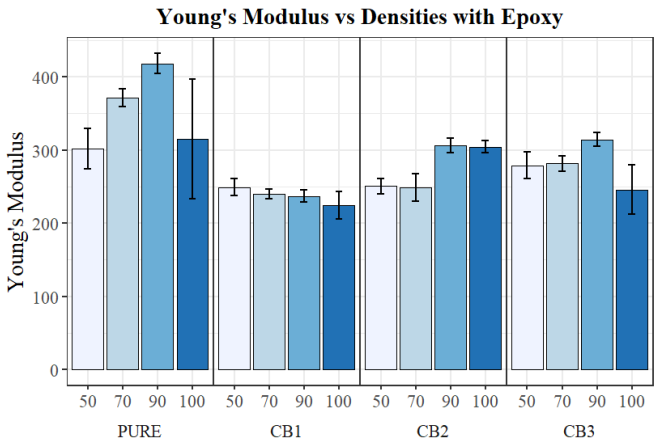

Figure 2. Variation of Young's modulus as a function of infill density for pure and CB-reinforced PLA/Epoxy composites

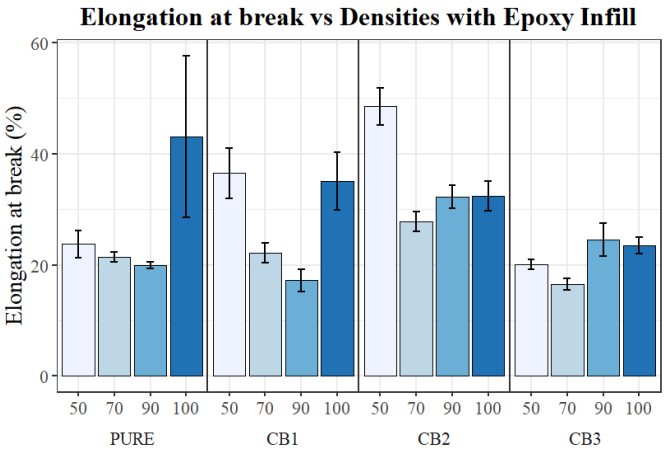

Figure 3. Variation of elongation at break as a function of infill density for pure and CB-reinforced PLA/Epoxy composites

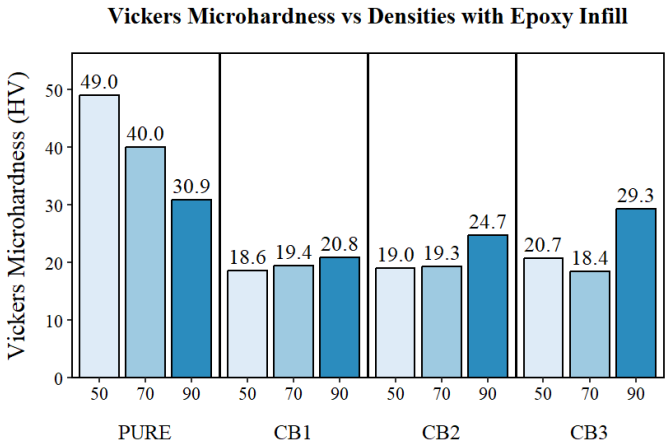

Figure 4. Variation of Vickers microhardness as a function of infill density for pure and CB-reinforced PLA/Epoxy composites

An elevated concentration of 3 wt% resulted in embrittlement at reduced densities, with CB3 elongation decreasing to 16.5 at 70% density specimen. The embrittling effect is a common issue when fillers aggregate, creating critical defect locations [7]. These results indicate that the 2 wt% rCB represents an optimal concentration for maximizing the toughening benefits of the epoxy-infilled composite system.

5.1.4. Hardness

The Vickers microhardness results (Figure 4) demonstrate complex trends across varying concentrations of rCB and infill densities. An inverse relationship was noted for pure PLA samples, with hardness diminishing from 49 HV at 50% density to 30.9 HV at 90% density. This phenomenon is ascribed to the efficacy of epoxy infiltration at 50% infill; the highly porous architecture enables significant penetration, resulting in an epoxy-rich surface layer. Considering that the cured epoxy resin generally demonstrated a superior hardness value (80 to 90HV) relative to the PLA_CB based 3D-printed samples (10–15 HV), the surface characteristics at low infill densities are predominantly influenced by the more rigid thermoset phase. At 90% infill, the diminished void volume restricts infiltration depth, which leads to a compositional alteration where the surface is increasingly characterized by the softer PLA matrix.

The integration of rCB significantly modifies this behavior, resulting in a substantial decrease in hardness (softening effect) at low concentrations. Samples containing 1 wt% rCB loading (CB1) demonstrated hardness values ranging from 18.6 to 20.8 HV across all densities, representing a reduction of up to 62% relative to pure PLA. This decrease is likely due to the hydrophobic characteristics of rCB, which obstruct epoxy wetting and hinder the development of the solid, epoxy-rich surface layer seen in pure samples. Additionally, at low concentrations, the rCB particles function as structural flaws or stress concentrators, augmenting surface porosity and diminishing resistance to indentation.

A notable enhancement in hardness was observed for samples containing 3 wt% rCB at 90% density, achieving 29.3 HV. This suggests that increased filler concentrations offer advantageous reinforcement when the structure is adequately dense to facilitate the development of a percolating filler network. At this 3 wt% threshold, the rCB particles attain adequate proximity to effectively limit polymer chain mobility and disperse loads, substantially offsetting the diminished epoxy infiltration at elevated densities. These findings indicate that surface microstructure, rather than solely bulk density, dictates the hardness characteristics of these hybrid composites.

5.2. Electrical Properties

The electrical impedance (Z) measurements (Figure 5) at 1000 Hz for the epoxy-infilled PLA-CB composite samples exhibit a non-monotonic relationship between rCB content and electrical performance. The PURE sample exhibited a baseline impedance of 341.84 MΩ. Upon the incorporation of 1 wt% rCB (CB1), the impedance increased by 25.2% to 427.85 MΩ, and reached 424.80 MΩ at 3 wt% (CB3). This U-shaped behavior indicates that the electrical properties are influenced by the interaction of filler distribution, percolation effects, and the dual-phase characteristics of the infilled structure.

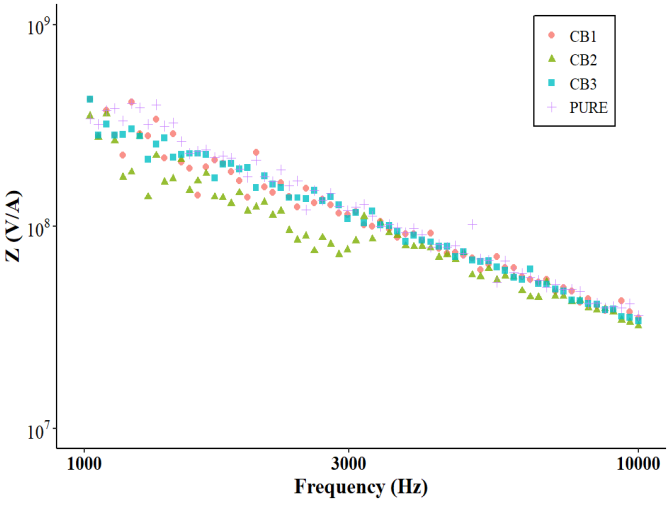

Figure 5. Impedance testing of PLA/CB infilled with epoxy at 50% density

The impedance spike at 1 wt% loading indicates sub-percolation activity. At this concentration, rCB particles are inadequately concentrated to create continuous pathways, existing instead as discrete conductive islands that disrupt polymer chain organization and form an interfacial polarization zone (Maxwell-Wagner-Sillars effect). These zones function as insulating barriers that hinder charge transport more than in the unfilled system.

The notable decrease in impedance at 2 wt% indicates that this composition nears the percolation threshold, wherein conductive particles start to create an interconnected network that enhances electron transport. This observation is consistent with classical theory regarding carbon black in thermoplastic matrices, which generally forecasts a threshold between 1 and 5 wt%. The unexpected increase noted at 3 wt% is attributed to particle agglomeration. Excessive loading leads to clustering, diminishing the effective surface area for conduction and forming insulating, polymer-rich domains. Moreover, excess rCB may interfere with the epoxy infilling process, which can result in an additional interfacial barrier between the PLA_CB matrix and the epoxy phase [8].

The recycled nature of the filler introduces additional complexity, as the rCB contains residual contaminants and variable particle sizes that may impede consistent network formation in comparison to virgin carbon black. Furthermore, the 3D printing process induces anisotropy, as the extrusion flow can align rCB particles along the printing direction, potentially diminishing conductivity perpendicular to the layers. The dual-phase architecture formed by the insulating epoxy infill establishes a system of competing pathways, wherein the epoxy occupies structural voids while concurrently introducing insulating barriers that the conductive PLA_CB phase must pass through. These findings underscore the need to optimize filler concentration and processing parameters to maintain the delicate equilibrium between conductive network formation and microstructural disruption.

5.3. Morphological and Chemical Analysis

5.3.1. Fourier Transform Infrared Spectroscopy (FTIR)

The Fourier Transform Infrared (FTIR) spectroscopy (Figure 6) confirmed the chemical stability and phase integration of the hybrid composites. The spectra validated that the fundamental polymer structure of PLA was preserved, as indicated by the distinctive carbonyl group (C=O) peak at about 1745 cm^{-1} and aliphatic hydrocarbons (CH_3 and CH) indicated by C-H stretching at 2918 cm^{-1} and bending at around 1456 cm^{-1} respectively. The absence of new chemical signatures suggests that the combination of components was primarily physical, thereby maintaining the chemical stability of the thermoplastic matrix throughout processing. The effective penetration and cross-linking of the epoxy resin within the 3D-printed samples were demonstrated by various diagnostic fingerprints.

The appearance of aromatic C=C skeletal peaks at 1606 cm^{-1} and 1508 cm^{-1} (Bisphenol A rings) and the C–O–C ether linkage at 1242 to 1244 cm^{-1} supports the development of a rigid, cross-linked structural backbone. A notable decrease in transmittance in the 1508 cm^{-1} aromatic band (from 92% to 86%) in rCB-reinforced samples indicates that CB functions as a structural reinforcement, enhancing localized resin density at the filler-matrix interface. The total elimination of hydroxyl (O–H) stretching peaks around 3200 to 3600 cm^{-1} in the infiltrated samples demonstrates that the resin effectively seals internal voids and displaces adsorbed moisture, which is crucial for preventing moisture thus it induced degradation and ensuring a compatible interface between the PLA shell and the epoxy core. Table 2 shows various functional groups involved in the chemical integration of the epoxy resin with the carbon black filler.

5.3.2. Optical Microscopy

Optical microscopy (OM) was used to examine the cross-sectional fracture surfaces to investigate the mechanical and electrical mechanisms of the hybrid composites. As observed in Figure 7(a), the neat epoxy resin completely penetrates the 3D-printed PLA macro-voids in the control specimen, demonstrating a clear dual-phase architecture and efficient fluid infiltration into the internal channels during the 36-hour room-temperature curing period. This secondary epoxy phase was modified by adding recycled carbon black (CB), as shown in Figures 7(b) and 7(c). The filler shows an ideal homogeneous dispersion without phase separation at 2wt% CB, as seen in Figure 7(c), creating continuous filamentary contact routes across the internal boundaries that optimize macroscopic electrical conductivity [12].

A highly textured, rigid core network that limits polymer chain mobility and maximizes load transfer efficiency is produced by increasing the filler content to 3 wt% CB, as shown in Figure 7(d). This microstructural density confirms the use of a 90% infill density which offers the required volumetric clearance to accommodate the viscous filler without creating microcracks, and directly explains the peak mechanical properties attained 21.9 MPa tensile strength and 29.3 HV hardness. However, substantial CB micro-agglomeration caused by particle self-affinity is also

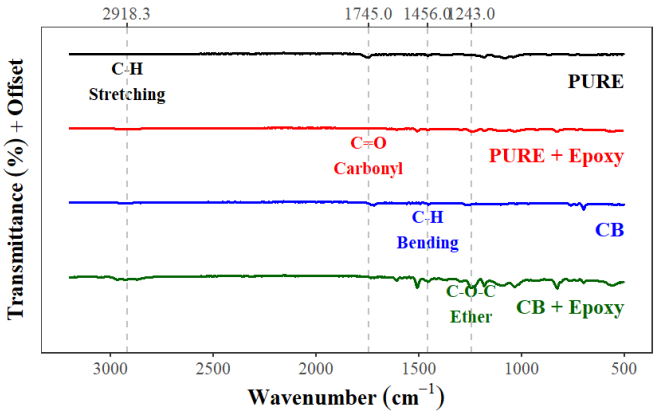

Figure 6. FTIR spectra of Pure, Pure + Epoxy, CB, and CB + Epoxy samples, illustrating the characteristic functional groups and chemical integration of the epoxy resin with carbon black filler

Table 2. Various functional groups involved in the chemical integration of the epoxy resin with the carbon black filler

Wavelength	Name of Functional Group	Summarized Purpose / Interpretation	Citation
~1745 cm^{-1}	Carbonyl group (C=O)	Confirms PLA structure is preserved; indicates physical blending and chemical stability.	[9]
2918 cm^{-1} ~1456 cm^{-1}	Aliphatic hydrocarbons (C–H stretching)	Confirms preservation of the baseline PLA polymer matrix.	[9]
1606 cm^{-1} & 1508 cm^{-1}	Aromatic C=C skeletal rings	Verifies epoxy resin penetration and the development of a rigid, cross-linked backbone. Decreased transmittance (92% to 86%) shows that rCB increases the localized resin density at the filler-matrix interface.	[10]
1242–1244 cm^{-1}	C–O–C ether linkage	Confirms effective epoxy cross-linking and structural backbone formation.	[10]
3200–3600 cm^{-1}	Hydroxyl group (O–H stretching)	Total elimination confirms that the epoxy resin seals internal voids and displaces moisture, preventing degradation.	[11]

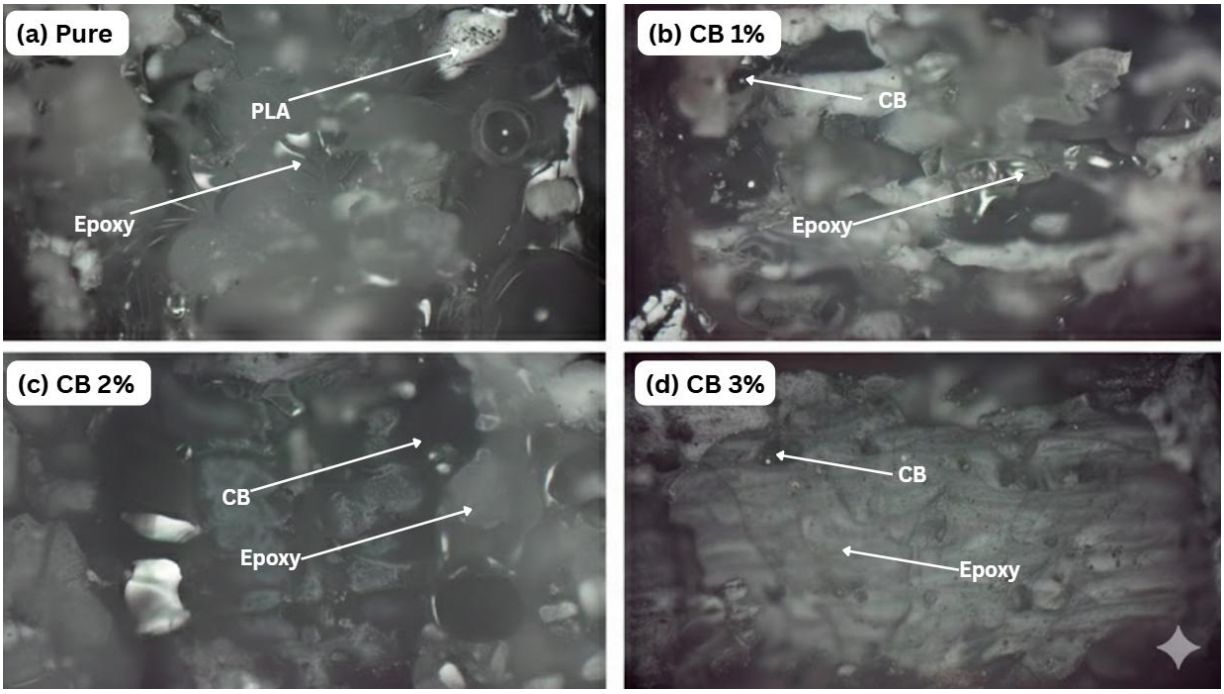

Figure 7. Microscopic morphology of PLA/Epoxy/CB composites: (a) Pure, (b) CB 1, (c) CB 2, (d) CB 3 at 90% infill density under 5x magnification

shown in Figure 7(d). By forming physical gaps and isolated high-resistance islands, this clumping behavior disrupts the continuous network and explains the clear trade-off where 3 wt% loading enhances mechanical reinforcement but significantly impairs electrical continuity [13]. In future work, SEM analysis will be conducted to better understand the morphology and dispersion of the filler within the matrix during melt compounding and to study the influence of the epoxy within the 3D-printed specimens.

6. CONCLUSION

This research shows the potential of enhancing 3D-printed PLA structures through the integration of recycled carbon black (rCB) reinforcement and secondary epoxy infiltration. The experimental results demonstrate that a 90% infill density serves as the optimal threshold for mechanical load-bearing, as fully dense (100%) structures suffer from processing-induced flaws and thermal stress. The 3 wt% rCB loading exhibited the highest tensile strength (21.9 MPa) and surface hardness (29.3 HV) due to the formation of effective percolating networks that enhance load transfer efficiency.

Nonetheless, the electrical performance necessitates careful adjustment of filler concentration; while 2 wt% rCB seems to be the optimal threshold for preserving continuous conductive pathways, elevated loadings (3 wt%) result in particle agglomeration and heightened resistance. Morphological investigation by FTIR established that the incorporation of epoxy and rCB was predominantly physical, maintaining the chemical stability of the PLA matrix while efficiently sealing internal spaces to avert moisture-induced deterioration. The interplay between the geometry of the 3D-printed scaffold and the epoxy infill results in a dual-phase architecture that harmonizes structural robustness with functional electrical characteristics. This hybrid manufacturing method offers a solid framework for producing sustainable, high-performance composites for the electronics sector.

ACKNOWLEDGMENTS

The authors would like to thank the Ministry of Higher Education (MoHE) Malaysia for the financial support provided through the Fundamental Research Grant Scheme (FRGS/1/2024/TK09/UNIMAP/02/21). Special thanks to Special appreciation are extended to Ecopower Synergy Sdn. Bhd. for supplying the recycled carbon black (rCB), which was a critical component of this research.

REFERENCES

[1] M. A. Tan, C. K. Yeoh, P. L. Teh, N. A. A. Rahim, C. C. Song, and C. H. Voon, "Effect of zinc oxide suspension on the overall filler content of the PLA/ZnO composites and cPLA/ZnO composites," *e-Polymers*, vol. 23, no. 1, 2023, doi: 10.1515/epoly-2022-8113.

[2] C. L. Custodio, P. J. M. Broñola, S. R. Cayabyab, V. U. Lagura, J. R. Celorico, and B. A. Basilia, "Powder Loading Effects on the Physicochemical and Mechanical Properties of 3D Printed Poly Lactic Acid/Hydroxyapatite Biocomposites," *International Journal of Bioprinting*, vol. 7, no. 1, p. 326, 2024, doi: 10.18063/ijb.v7i1.326.

[3] D. Dou *et al.*, "Optimization of 3D Printing Parameters of Polylactic-Co-Glycolic Acid-Based Biodegradable Antibacterial Materials Using Fused Deposition Modeling," *3D Printing and Additive Manufacturing*, vol. 11, no. 3, pp. 1343–1355, 2024, doi: 10.1089/3dp.2022.0340.

[4] R. Fidalgo-Pereira *et al.*, "Effect of inorganic fillers on the light transmission through traditional or flowable resin-matrix composites for restorative dentistry," *Clinical Oral Investigations*, vol. 27, no. 9, pp. 5679–5693, 2023, doi: 10.1007/s00784-023-05189-7.

[5] P. C. Leow *et al.*, "Effect of Silicone Rubber on the Properties of Epoxy/Recovered Carbon Black (rCB) Conductive Materials," *International Journal of Nanoelectronics and Materials (IJNeaM)*, vol. 17, no. 2, pp. 270–278, 2024, doi: 10.58915/ijneam.v17i2.705.

[6] Noor. H. Majeed, "Mechanical and Thermal Behavior of Epoxy Composites with Carbon Black," *Academia Open*, vol. 10, no. 2, 2025, doi: 10.21070/acopen.10.2025.13102.

[7] R. Mandala, B. A. Prasad, and S. Akella, "Development and characterization of groundnut shell-derived biocarbon-reinforced polylactic acid composite filaments for FDM," *Journal of Applied Polymer Science*, vol. 141, no. 30, 2024, doi: 10.1002/app.55689.

[8] J. Mogan *et al.*, "Fused Deposition Modelling of Polymer Composite: A Progress," *Polymers*, vol. 15, no. 1, p. 28, 2022, doi: 10.3390/polym15010028.

[9] K. Nath, S. Ghosh, S. K. Ghosh, P. Das, and N. Ch. Das, "Facile preparation of light-weight biodegradable and electrically conductive polymer based nanocomposites for superior electromagnetic interference shielding effectiveness," *Journal of Applied Polymer Science*, vol. 138, no. 22, 2021, doi: 10.1002/app.50514.

[10] H. Özer, "Infiltration-Assisted Mechanical Strengthening of 3D-Printed Polypropylene Lattice and Thin-Walled Tube Structures," *Polymers*, vol. 17, no. 19, p. 2604, 2025, doi: 10.3390/polym17192604.

[11] I. Plamadiala, C. Croitoru, M. A. Pop, and I. C. Roata, "Enhancing Polylactic Acid (PLA) Performance: A Review of Additives in Fused Deposition Modelling (FDM) Filaments," *Polymers*, vol. 17, no. 2, p. 191, 2025, doi: 10.3390/polym17020191.

[12] L. Sandanamsamy *et al.*, "A comprehensive review on fused deposition modelling of polylactic acid," *Progress in Additive Manufacturing*, vol. 8, no. 5, pp. 775–799, 2023, doi: 10.1007/s40964-022-00356-w.

[13] S. Thumsorn, W. Prasong, T. Kurose, A. Ishigami, Y. Kobayashi, and H. Ito, "Rheological Behavior and Dynamic Mechanical Properties for Interpretation of Layer Adhesion in FDM 3D Printing," *Polymers*, vol. 14, no. 13, p. 2721, 2022, doi: 10.3390/polym14132721.

[14] Q. Wei, R. Yang, X. Zhao, J. Zhou, Y. An, and S. Yang, "Fused deposition modeling of carbon-reinforced polymer matrix composites: A comprehensive review," *Polymer Composites*, vol. 44, no. 9, pp. 5313–5345, 2023, doi: 10.1002/pc.27498.

[15] L. Wenjing, S. Xu, and Z. Yanbin, "Study of PLA/TPU/Sodium Lignosulfonate Composite for Eco-Friendly 3D Printing of Wood-Like Materials," *Journal of Applied Polymer Science*, vol. 143, no. 6, 2026, doi: 10.1002/app.58198.